Available online at www.sciencedirect.com
ScienceDirect
Journal of Power Sources 163 (2006) 166–172
JOURNAL OF POWER SOURCES
www.elsevier.com/locate/jpowsour

Eutectic self-mixing method for the preparation of $LiMn_2O_4$ without any artificial mixing procedures

Hyun-Koo Kang [a], Wook Ahn [a], Seung-Goo Lee [a], Kyoo-Seung Han [a,*], Jun-Ho Song [b], Oh-Heon Kwon [b], Eun-Young Kang [b]

[a] *Division of Advanced Materials Engineering, Chungnam National University, Daeduk Science Town, Taejeon 305-764, South Korea*
[b] *JES·E·CHEM Corp., Shihung 429-450, South Korea*

Received 20 August 2005; received in revised form 19 May 2006; accepted 27 May 2006
Available online 24 July 2006

Abstract

Spinel $LiMn_2O_4$ as a cathode material for lithium rechargeable batteries is economically prepared by a novel eutectic self-mixing method without any artificial mixing procedures of reactants. The phase transitions of lithium manganese oxide are found three times on the preparation. Thus, those process controls are discussed and emphasized. The prepared $LiMn_2O_4$ exhibits the initial discharge capacity of 124.8 mAh g^{-1} and the discharge capacity retention of 98.2% after 20 cycles.

Keywords: Eutectic self-mixing method; $LiMn_2O_4$; Lithium rechargeable battery; Cathode

1. Introduction

Spinel phase $LiMn_2O_4$ has been studied extensively as a cathode material for lithium rechargeable batteries. Spinel $LiMn_2O_4$ offers considerable advantages in high cell voltage with much lower cost as compared to $LiCoO_2$ and $Li_{1-x}Ni_{1+y}O_2$. However, $LiMn_2O_4$ has a lower capacity and suffers from a capacity loss upon cycling. To improve the electrochemical properties of the spinel phase $LiMn_2O_4$, several research groups have studied using various synthetic methods. The most widely used method for the preparation of $LiMn_2O_4$ is the direct reaction, in the solid state, of a mixture of solid reactants at high temperature. It is usually called as solid-state chemistry reaction [1–5]. In the solid-state chemistry reaction, however, mixing procedures of solid reactants by pulverization and/or grinding must be applied for complete reaction. In the scaling up production of cathode materials, cost of mixing procedures increases exponentially. Furthermore, an agglomeration procedure of the pulverized and/or grinded solid reactants is also required for the amelioration of the contact across a shared face of reactants. Other techniques include molten salt method, sol–gel method, and hydrothermal method [6–11]. The molten salt method avoids the pulverization and grinding of reactants if the morphology and particle size of solid reactants are optimized for complete reaction. Unfortunately, morphology and particle size controls are much more difficult than pulverization and grinding. In the sol–gel method, the dissolved ion species are spontaneously mixed. Thus, we do not need to pulverize, grind, and agglomerate the solid reactants. However, although solvents are not compositional elements of $LiMn_2O_4$, the usage and the evaporation of solvents are indispensable in sol–gel method. Those require additional material and energy consumption. To overcome these synthetic disadvantages, we develop a novel eutectic self-mixing method to accomplish homogeneous mix of molten reactants without any artificial mixing procedures. When two low-temperature melting compounds, $LiCH_3CO_2{\cdot}2H_2O$ (m.p.: 59 °C) and $Mn(CH_3CO_2)_2{\cdot}4H_2O$ (m.p.: 67 °C), are exposed to a temperature above their eutectic points, they exist as typical fluidic forms that are capable of being mixed. Spinel phase $LiMn_2O_4$ is economically prepared using this method, spontaneous mixing at eutectic state and direct thermal reaction, without any pulverization, grinding, agglomeration, morphol-

* Corresponding author. Tel.: +82 42 821 5897; fax: +82 42 822 6637.
E-mail address: kshan@cnu.ac.kr (K.-S. Han).

0378-7753/$ – see front matter © 2006 Elsevier B.V. All rights reserved.
doi:10.1016/j.jpowsour.2006.05.042

ogy controlling, particle size controlling, and even artificial stirring of the reactants.

2. Experimental

2.1. Materials

Both $LiCH_3CO_2{\cdot}2H_2O$ and $Mn(CH_3CO_2)_2{\cdot}4H_2O$ were simultaneously and homogeneously dropt on alumina vessel with those molar ratio of 1.05–2.0. Without any pulverization, grinding, and even artificial stirring of the metal acetates, the reactants were consecutively heated up to their eutectic temperature (70 °C) for 40 min, 250 °C for 8 h, and 750 °C for 20 h at a rate of 10 °C min^{-1} in air without any intermittent cooling. Excess $LiCH_3CO_2{\cdot}2H_2O$ was used to compensate for the loss of Li during the heating. The heating at 250 °C before the calcinations at 750 °C is needed to obtain the steady phase transitions. This point will be discussed in detail. Several intermediates were also prepared to investigate the phase changes during the preparation of $LiMn_2O_4$ by the eutectic self-mixing method. The synthetic conditions and the names on samples are listed in Table 1.

In addition, two spinel phases $LiMn_2O_4$ are independently prepared by sol–gel method and solid-state chemistry reaction. The preparation of $LiMn_2O_4$ using sol–gel method was following: 0.105 mol of $LiCH_3CO_2{\cdot}2H_2O$ and 0.2 mol of $Mn(CH_3CO_2)_2{\cdot}4H_2O$ were dissolved in doubly distilled water and mixed with acrylic acid solution (10%). Nitric acid solution (7%) was then slowly dripping in the solution with constant stirring at room temperature up to pH 2. The resulting solution was mixed with constant stirring at 80 °C to obtain a clear viscous gel. The gel was dried in a vacuum oven at 100 °C for 10 h. The dried gel was the first heated at 400 °C for 1 h in air. The second heat treatment for 24 h was performed with intermittent cooling and grinding procedures at 750 °C in air.

In the preparation using the solid-state chemistry reaction, 0.15 mol of Li_2CO_3 and 0.6 mol of MnO_2 were ground together and then put on alumina vessel. The successive heat treatments of mixture have been performed with intermittent cooling and grinding procedures at 450 °C for 12 h and 750 °C for 24 h in air.

Table 1
Heating temperatures and reaction times to prepare the samples as well as their designations

Label	Heating temperature and reaction time
M1	70 °C, 5 min
M2	70 °C, 10 min
M3	70 °C, 40 min
M4	70 °C, 40 min + 170 °C, 10 min
M5	70 °C, 40 min + 250 °C, 10 min
M6	70 °C, 40 min + 250 °C, 2 h
M7	70 °C, 40 min + 250 °C, 8 h
M8	70 °C, 40 min + 250 °C, 8 h + 300 °C, 10 min
M9	70 °C, 40 min + 250 °C, 8 h + 400 °C, 10 min
M10	70 °C, 40 min + 250 °C, 8 h + 750 °C, 20 h
NE–$LiMn_2O_4$	750 °C, 20 h

The reactants are $LiCH_3CO_2{\cdot}2H_2O$ and $Mn(CH_3CO_2)_2{\cdot}4H_2O$.

2.2. Characterization

Thermal analysis of the acetates was performed at a rate of +1 °C min^{-1}, from room temperature to 1000 °C, in air using SDT 2960 TG–DTA (TA Instruments). Elemental analysis of the prepared lithium manganese oxides was carried out by ICP-AES (Jobin Yvon, JY38S) and Carlo Erba EA 1108 CHN analyzer. ^{7}Li NMR measurements were carried out at room temperature on Bruker DSX 400 with a 9.4 T magnet. Magic angle spinning (MAS) NMR experiments were performed using a 4 mm CP-MAS probe and zirconia sample rotor. The ^{7}Li resonance frequency used was 155.6 MHz; a sample spinning speed of 14 kHz was employed. Spectra were acquired using single-pulse and echo-pulse sequences. Both quadrupolar echoes and spin-echoes were used to acquire spectra of all samples. However, the spectra were subsequently acquired with echo-pulse sequences to ensure that no resonances were missed with single-pulse sequence. All spectra were referenced to an external 1 M LiCl solution; a 90° pulse-length of 4.3 μs, repetition delay of 0.1 s, and spectral width of 0.7 MHz were used. For enhancement of spectral resolution, 256–20,000 acquisitions were used. The acquired spectra, with their complex spinning sideband manifolds, were difficult to use to derive isotropic chemical shifts. The problem due to the uncertainties in phasing the spectra was overcome by performing the experiments at several MAS speeds; each spectrum could be phased by inter comparison. Room-temperature Raman measurements were performed using a Jobin Yvon/Atago Bussan T64000 triple spectrometer. The spectral resolution was 2–3 cm^{-1}. Elemental analysis of the prepared phases was carried out by ICP-AES (Jobin Yvon, JY38S) and Carlo Erba EA 1108 CHN analyzer. X-ray diffraction (XRD) pattern analyses were achieved by using a Mac Science M03XHF[22] diffractometer and Cu Kα radiation (λ = 1.5405 Å) operated with 30 mA and 40 kV. The diffractograms were recorded in the 2θ range of 5–90° with 0.02° intervals at a scanning rate of 2° min^{-1}. Mn K-edge X-ray absorption spectroscopy (XAS) data were obtained using the BL7C1 beam-line of Pohang Light Sources (PLS). Synchrotron radiation from the electron storage ring (2.5 GeV with about 120–170 mA of stored current) was monochromatized with a Si(3 1 1) double-crystal monochromator. All Mn K-edge XAS data were collected in transmission mode at room temperature. Absorbance was measured with the ionization chamber filled with N_2 (85%) + Ar (15%) and N_2 (100%) for incident and transmitted beams, respectively. The high order harmonics have been eliminated with detuning to 70% of incident beam intensity. The monochromatic X-ray beam has been used with the energy resolution ($\Delta E/E$) below 2×10^{-4}. The energy of each spectrum was calibrated from the energy scale of the Mn metal spectra. To remove the energy shift problem, the X-ray absorption spectrum for the metal foil has been measured simultaneously in every measurement as the metal foil was positioned in front of the window of the third ion chamber. The absorbance $\mu(E)$ was normalized to an edge-jump of unity to compare the X-ray absorption near-edge structure (XANES) features directly with one another. The EXAFS data analyses have been carried out by the standard procedure elsewhere. The measured absorption spectra below the pre-edge region was fitted to a straight line, and

then the background contribution above the post-edge region, $\mu_0(E)$, was fitted to a high order polynomial. The fitted polynomials have been extrapolated through the total energy region and subtracted from the total absorption spectra. The background-subtracted absorption spectra were normalized for the above energy region, $\chi(E) = \{\mu(E) - \mu_0(E)\}/\mu_0(E)$. The normalized k^3-weighted EXAFS spectra, $k^3\chi(k)$, have been Fourier transformed in the k range from 2.0 to 14.0 $Å^{-1}$ with the hanning window function in order to show the contribution of each bond pair on the Fourier transform (FT) peak. Electrochemical tests were carried out at room temperature using coin cells. The prepared cathode materials were mixed with 7 wt.% super-P carbon black and 8 wt.% poly-vinylidene fluoride (PVDF) binder dissolved in *N*-methyl-2-pyrrolidone (NMP) until a slurry was obtained. The slurry was laminated on an Al foil using a hot-roller press. The electrolyte was a 1.0 M solution of $LiPF_6$ in ethylene carbonate (EC) and ethyl methyl carbonate (EMC) with 1:2 volume ratio. Lithium foil was used as anode; cell assembly was performed in an Ar-filled glove box; cells were charged and discharged at *C*/5.

3. Results and discussion

TG–DTA curves in Fig. 1 ascertain that the first weight-loss (29.8%) between room temperature and 170 °C together with small endothermic DTA peaks around 100 °C correspond to the removal of hydrated $10H_2O$ (30.4%). Beyond 170–250 °C, decomposition of lithium acetate and manganese acetate results in the second weight loss of 38.8% and two large exothermic DTA peaks around 250 °C. This result agrees well with the calculated value, 39.0% for the release of $7.5H_2O$ and $10CO_2$, as well as the gain of $10.75O_2$. The reaction pathway can thus be given as follows:

$$LiCH_3CO_2{\cdot}2H_2O + 2Mn(CH_3CO_2)_2{\cdot}4H_2O \rightarrow LiMn_2(CH_3CO_2)_5 + 10H_2O \quad (1)$$

$$LiMn_2(CH_3CO_2)_5 + 10.75O_2 \rightarrow LiMn_2O_4 + 7.5H_2O + 10CO_2 \quad (2)$$

The decomposition of both acetates around 250 °C releases massive heat. This exothermic heat is predicted to be utilized as the lattice energy required for the formation of $LiMn_2O_4$ phase. Usually, the lattice energy is supplied by external heating. The temperature of 250 °C is the end-point for thermal weight loss, which means it is possible to prepare $LiMn_2O_4$ phase at a low temperature around 250 °C. This is another advantage of the eutectic self-mixing method. Although the synthetic method of "low-temperature $LiMn_2O_4$" at the 400–450 °C range has been previously reported [2–4,12–15], there has been no reports on a synthetic way to prepare pure spinel $LiMn_2O_4$ phase below the temperature of 250 °C. The detailed results about the $LiMn_2O_4$ phase prepared at 250 °C using the eutectic self-mixing method will be discussed elsewhere.

An evidence for the spontaneous and homogeneous mixing during the eutectic self-mixing preparation can be obtained by ICP-AES and CHN analysis of the M7 and M10. Unless the molten acetates are homogeneously mixed, the M7 and M10 samples should contain lithium carbonate and/or manganese carbonate. It means the M7 and M10 phases should have abundant carbon. Actually, the M7 and M10 phases are seen to contain no carbon. In addition, the chemical composition of the prepared $LiMn_2O_4$ phases was obtained by the ICP-AES results. Those relative Li and Mn molar ratios, calculated from the ICP-AES results, were evaluated to 0.98:1.00 (M10), 0.94:1.00 (sol–gel method), and 0.97:1.00 (solid-state chemistry reaction).

The ^{7}Li MAS NMR spectroscopy has been used to study the changes in the local environments of lithium during the preparation of $LiMn_2O_4$ using the eutectic self-mixing method. Fig. 2 shows the ^{7}Li MAS NMR spectra of thermally exposed reactants at various conditions. The spectrum of $LiCH_3CO_2{\cdot}2H_2O$ shows a sharp resonance having very weak spinning sidebands with an isotropic resonance at ~0 ppm. This is a typical spectrum of a normal diamagnetic solid solution. As shown in Fig. 2(b), the chemical environment of lithium in lithium acetate heated at 70 °C for 5 min remains unchanged. It confirms that the first weight-loss of 29.8% in the TG curve is on account of the removal of hydrated $10H_2O$, not as the decomposition of the acetates. However, the NMR spectra of M2 and M3 show significantly broadened isotropic line with the trivial chemical shift and the enhanced spinning sideband manifolds compared to those of $LiCH_3CO_2{\cdot}2H_2O$. The enhancement of spinning sideband manifolds with the increased heating time is caused by the increased portion of paramagnetic manganese around lithium, and the spectral line broadening is originated from the anisotropic bulk magnetic susceptibility [16,17]. These critical features indicate that the molten acetates in this synthetic procedure are mixed by themselves.

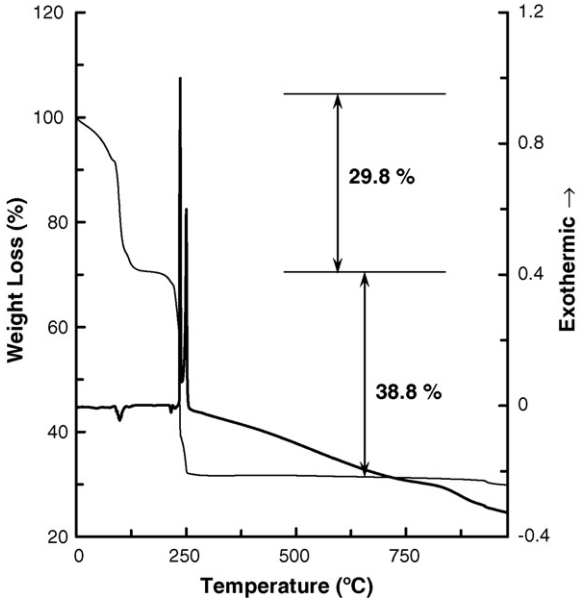

Fig. 1. TG–DTA curves of $LiCH_3CO_2{\cdot}2H_2O$ and $Mn(CH_3CO_2)_2{\cdot}4H_2O$ measured at a heating rate of 1 °C min^{-1} under an oxygen flow.

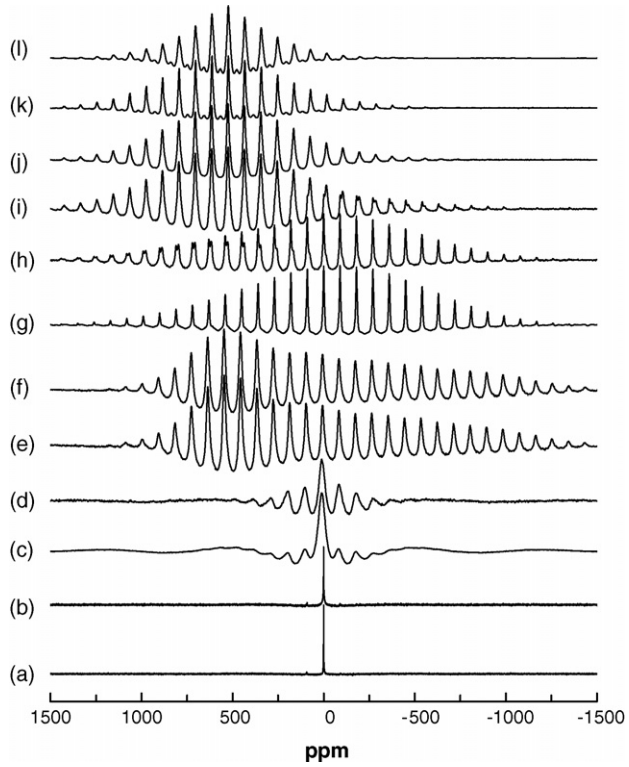

Fig. 2. ^{7}Li MAS NMR spectra of: (a) $LiCH_3CO_2{\cdot}2H_2O$, (b) M1, (c) M2, (d) M3, (e) M4, (f) M5, (g) M6, (h) M7, (i) M8, (j) M9 and (k) M10 prepared using eutectic method, and (l) $LiMn_2O_4$ phase prepared by solid-state chemistry reaction. All spectra were acquired at room temperature with spinning speeds of 14 kHz.

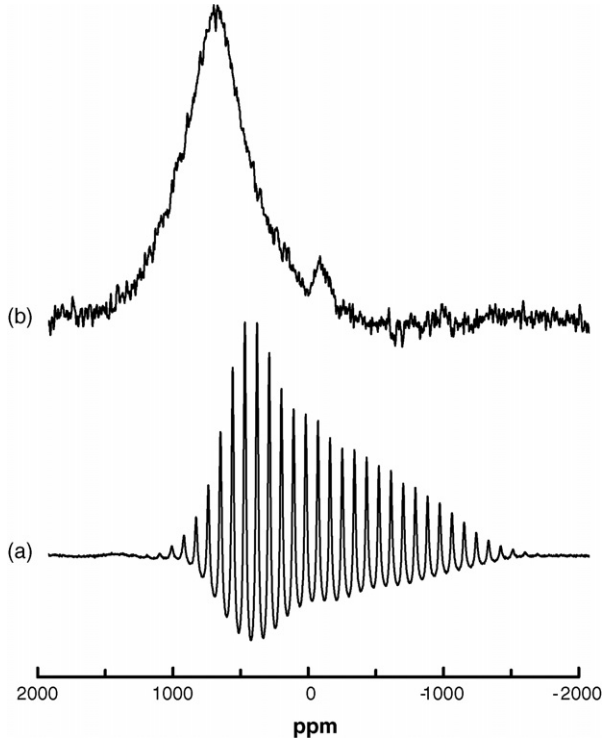

Fig. 3. ^{7}Li MAS NMR spectra of M5 with: (a) spinning speeds of 14 kHz and (b) static experiment.

Three characteristic features can be seen in the NMR spectra of M4 and M5; the abrupt isotropic shift moving to lower field, the markedly enhanced spinning sideband manifolds, and the drastically broadened spectral width. It is difficult to identify the isotropic resonance by MAS experiments; therefore, a static experiment (Fig. 3) was used to determine the isotropic chemical shift of 760 ppm. The Fermi contact shift by the interaction between the unpaired electron spins of manganese and nuclear spins of lithium causes the abrupt isotropic chemical shift of 760 ppm, and also explains the other characteristic features of spectra [18,19]. Thus, this dominant resonance can be assigned to the lithium, existed as an intermediate, in a lithium manganate (phase I). As shown in Fig. 3, relatively small portion of a characteristic resonance at ∼0 ppm is also observed, which results from the non-interacted lithium with manganese such as lithium acetate due to very short reaction time of 10 min for making a single phase I.

For the samples of M6 and M7, the resonance at 760 ppm is not apparent and an isotropic resonance at ∼0 ppm is detected as shown in Fig. 2(g) and (h). In ^{7}Li NMR, a resonance at ∼0 ppm is usually observed for a diamagnetic solid solution, such as lithium acetate. For the conditions of our experiment, this signal is expected due to rather decomposition of lithium acetate than diamagnetic solid solution. To verify the chemical environment of M6 and M7 having this unusual chemical shift, this sample was also analyzed by variable-temperature Raman spectroscopy and elemental analysis. The characteristic Raman peak of M7 in Fig. 4(g) is observed at 650 cm^{-1}, while the complicated Raman peaks of lithium acetate are observed. In the elemental analysis of M6, the wt.% of carbon was determined below system error. On the basis of these two results, it is obvious that lithium acetate or possible impurities such as lithium carbonate are not present in M6. Furthermore, it was found by iodometric titration that the average oxidation state of manganese in M6 is higher than that of spinel $LiMn_2O_4$ containing both Mn^{4+} and Mn^{3+} ions in a 1:1 ratio. Since the chemical shift of the ^{7}Li resonance for lithium manganate having Mn^{4+} is varying by the combination of semi-linear and bent (90°) Li–O–Mn bonds, it would be shifted to ∼0 ppm [19]. Therefore, the dominant resonance for M6 can be assigned to the lithium, existed as the second intermediate of lithium manganate (phase II), which is produced by the phase transition at the temperature of 250 °C. Also, a resonance at 523 ppm is observed in Fig. 2(g) and (h), which can be certainly assigned to lithium in the general position, 8a, of spinel $LiMn_2O_4$ structure by the Fermi contact shift mechanism as expected [19]. Therefore, all the lithium atoms under this condition are interacted with manganese, which directly indicates a successful homogeneous mixing of reactants through the eutectic self-mixing procedure. Incidentally, the heating at 250 °C for 8 h before the calcinations at 750 °C for 20 h is applied for the steady phase transitions.

For the samples of M7, M8, and M9, the portion of a resonance at 523 ppm compared to that at ∼0 ppm is successively enlarged as shown in Fig. 2(h)–(j), respectively, which clearly shows the additional transition from phase II to spinel $LiMn_2O_4$ with the increase of both reaction temperature and time.

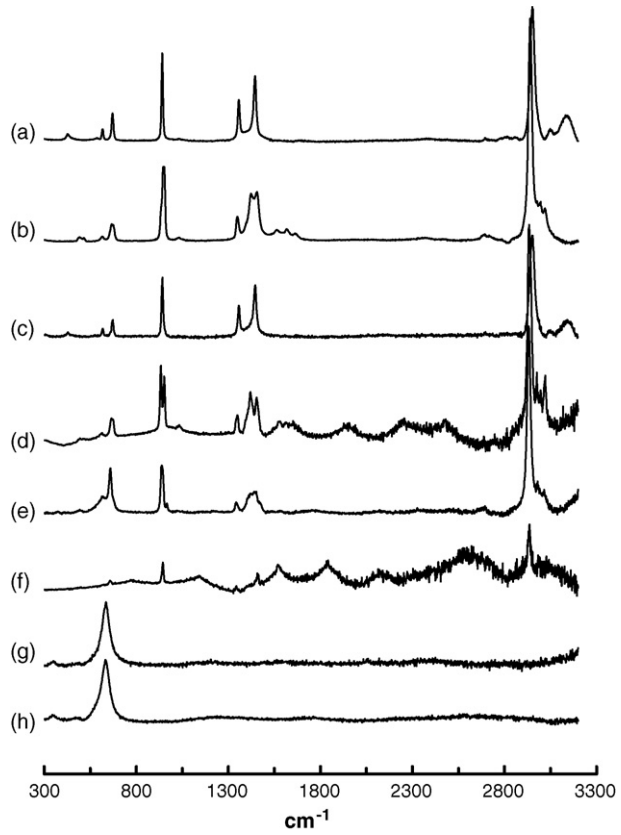

Fig. 4. Raman spectra of: (a) $LiCH_3CO_2{\cdot}2H_2O$, (b) $Mn(CH_3CO_2)_2{\cdot}4H_2O$, (c) M3, (d) M4, (e) M5, (f) M6, (g) M7 and (h) M10 prepared using eutectic self-mixing method.

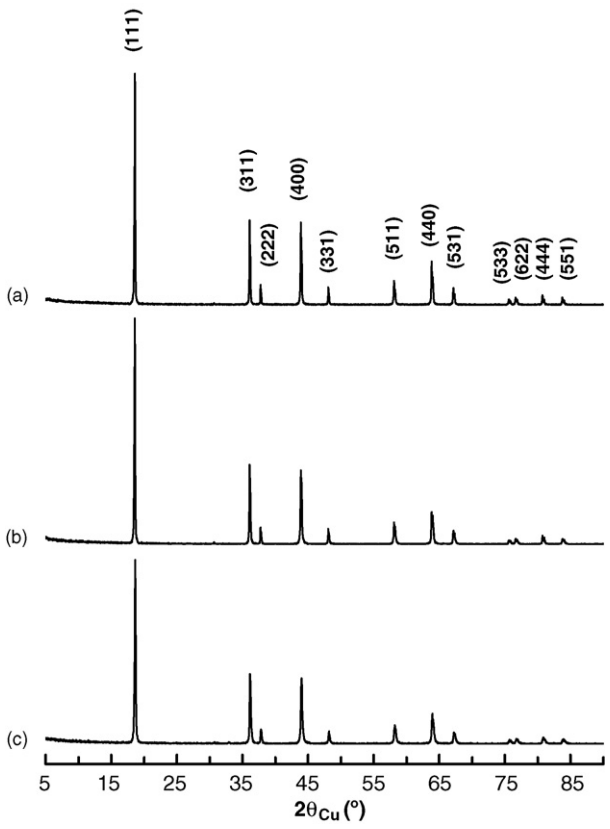

Fig. 5. X-ray diffraction patterns for spinel $LiMn_2O_4$ phases (space group: *Fd3m*) prepared by: (a) eutectic self-mixing method, (b) sol–gel method, and (c) solid-state chemistry reaction.

The spectrum of M10, sintered at 750 °C for 20 h, contains a resonance of spinel $LiMn_2O_4$ mainly at 523 ppm and an additional resonance weakly at 566 ppm, as shown in Fig. 2(k). The later is generally originated from the inevitable crystalline imperfections such as vacancies on both the lithium and manganese sites. These are consistent with the results previously reported by Morgan et al. [18] and Lee et al. [19]. In addition, the identical features between Fig. 2(k) and (l) indicate that spinel $LiMn_2O_4$ is successfully prepared by the eutectic self-mixing method.

The $LiMn_2O_4$ phases prepared by eutectic self-mixing method, sol–gel method, and solid-state chemistry reaction were characterized with respect to those macro and microstructures by the XRD pattern analysis and the XAS analysis, respectively. The XRD patterns are shown in Fig. 5. All XRD peaks of the prepared phases are characteristic for the space group *Fd3m* as spinel $LiMn_2O_4$ phase [20]. All of the prepared $LiMn_2O_4$ phases crystallize in the cubic system ($a = 8.247$ Å). In the XRD patterns of three $LiMn_2O_4$ phases, we cannot find any different features. Mn K-edge XAS spectra of the $LiMn_2O_4$ phases prepared by eutectic self-mixing method, sol–gel method, and solid-state chemistry reaction are shown in Figs. 6 and 7. Since the peak features are very sensitive to the oxidation state of the central Mn atom, the bond covalency, and the local structure around the Mn atom, the same appearances of the Mn K-edge XAS spectra of the $LiMn_2O_4$ phases prepared by eutectic self-mixing method,

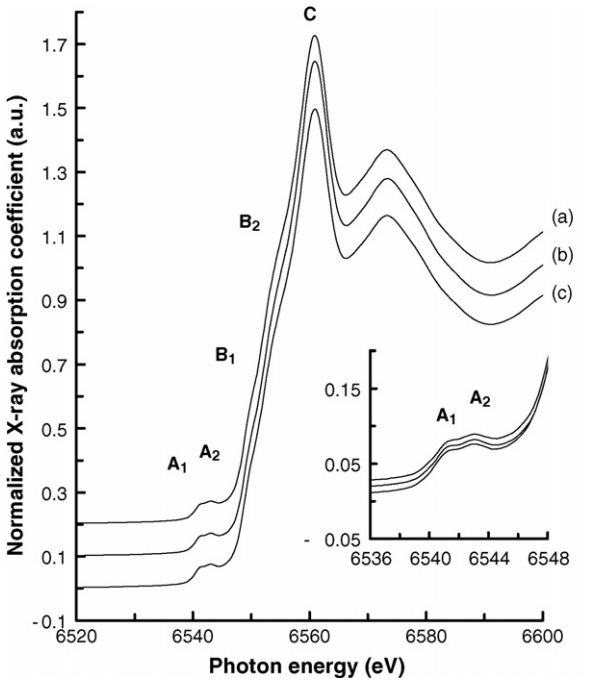

Fig. 6. Mn K-edge XANES spectra for spinel $LiMn_2O_4$ phases prepared by: (a) the eutectic self-mixing method, (b) sol–gel method, and (c) solid-state reaction.

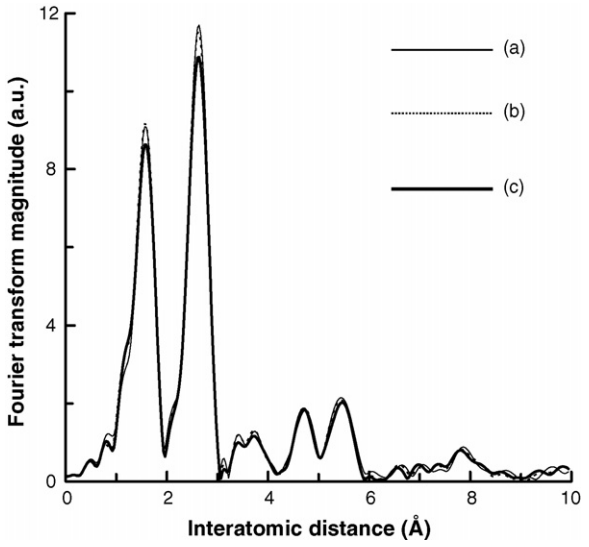

Fig. 7. Variations in Fourier transform magnitude of Mn K-edge EXAFS for spinel $LiMn_2O_4$ phases prepared by: (a) the eutectic self-mixing method, (b) sol–gel method, and (c) solid-state reaction.

sol–gel method, and solid-state chemistry reaction indicate that the Mn atoms in three $LiMn_2O_4$ phases are in the same physicochemical state. It also means that the $LiMn_2O_4$ phases prepared by eutectic self-mixing method, sol–gel method, and solid-state chemistry reaction have the same microstructure.

As shown in Fig. 8, the $LiMn_2O_4$ phase prepared by the eutectic self-mixing method exhibits the initial discharge capacity of 124.8 mAh g^{-1} and the discharge capacity retention of 98.2% after 20 cycles. However, the NE–$LiMn_2O_4$ phase prepared without the heating procedures of 70 °C for 40 min and 250 °C for 8 h exhibits the initial discharge capacity of 106.8 mAh g^{-1} and the discharge capacity retention of 22.2% after 20 cycles. The cycling performance of NE–$LiMn_2O_4$ is severely poor in comparison with that of the $LiMn_2O_4$ prepared using the eutectic self-mixing method, which directly represents the key role of the eutectic self-mixing and the phase translation procedures in the preparation of well-crystallized spinel $LiMn_2O_4$. Because $LiMn_2O_4$ is prepared through the slow but steady phase translation procedures using this method, its battery performances might be higher than those of the cathode materials prepared by other synthetic methods.

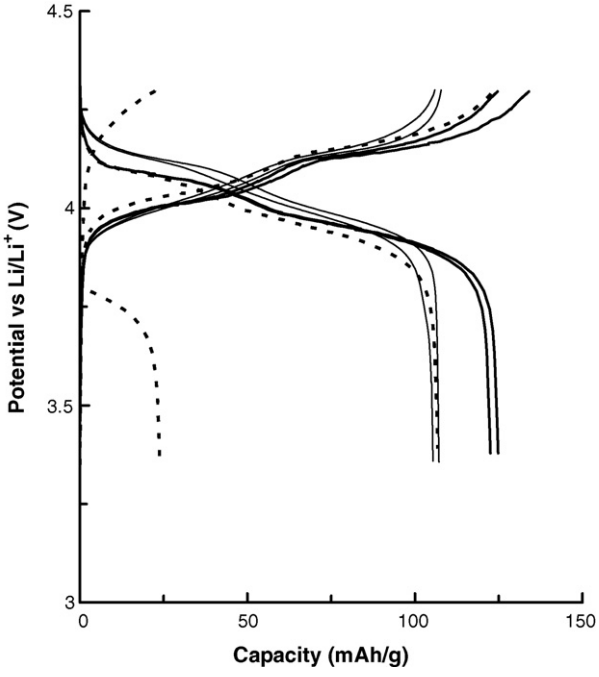

Fig. 8. Voltage vs. capacity profiles of 1st and 20th cycles for the $LiMn_2O_4$ phases prepared by the eutectic self-mixing method (▬) and the solid-state chemistry reaction (—), together with NE–$LiMn_2O_4$ (- - -).

4. Conclusion

Spinel $LiMn_2O_4$ as a cathode material for lithium rechargeable batteries is prepared by a novel eutectic self-mixing method without any artificial mixing procedure. The spontaneous and homogeneous mixes as well as the phase transitions on the preparation of spinel $LiMn_2O_4$ are demonstrated by ^7Li MAS NMR spectroscopy. The steady phase transition procedure during the eutectic self-mixing preparation results in the advanced discharge capacities of the materials prepared using this method. Furthermore, the usage of this method in the production of lithiated cathode materials will result in a decrease in production cost.

Acknowledgement

This work was funded by Korea Research Foundation Grant (KRF-12005-005-J00403) and BK21-E2M.

References

[1] Y. Gao, J.R. Dahn, J. Electrochem. Soc. 143 (1996) 100.
[2] C. Masquelier, M. Tabuchi, K. Ado, R. Kanno, Y. Kobayashi, Y. Maki, O. Nakamura, J.B. Goodenough, J. Solid State Chem. 123 (1996) 255.
[3] S. Choi, A. Manthiram, J. Electrochem. Soc. 147 (2000) 1623.
[4] J.P. Cho, M.M. Thackeray, J. Electrochem. Soc. 146 (1999) 3577.
[5] J.M. Tarascon, D. Guyomard, Electrochim. Acta 38 (1993) 1221.
[6] Y. Xia, M. Yoshio, J. Electrochem. Soc. 143 (1996) 825.
[7] Y.S. Lee, M. Yoshio, Electrochem. Solid-State Lett. 4 (2001) A85.
[8] W. Liu, G.C. Farrington, F. Chaput, B. Dunn, J. Electrochem. Soc. 143 (1996) 879.
[9] P. Barboux, J.M. Tarascon, F.K. Shokoohi, J. Solid State Chem. 94 (1991) 185.
[10] T. Kanasaku, K. Amezawa, N. Yamamoto, Solid State Ionics 133 (2000) 51.
[11] K.S. Han, S.W. Song, T. Watanabe, M. Yoshimura, Electrochem. Solid-State Lett. 2 (1999) 63.
[12] M.M. Thackeray, A. de Koch, M.H. Rossouw, D. Liles, R. Bittihn, D. Hoge, J. Electrochem. Soc. 139 (1992) 363.
[13] S.R.S. Prabaharan, B.S. Nasiman, S.S. Michael, M. Massot, C. Julien, Solid State Ionics 112 (1998) 25.
[14] T. Le Mercier, J. Gaubicher, E. Bermejo, Y. Chabre, M. Quarton, J. Mater. Chem. 9 (1999) 567.
[15] P. Mustarelli, V. Massarotti, M. Bini, D. Capsoni, Phys. Rev. B 55 (1997) 12018.

[16] W.P. Rothwell, J.S. Waugh, J.P. Yesinowski, J. Am. Chem. Soc. 102 (1980) 2637.
[17] A. Nayeem, J.P. Yesinowski, J. Chem. Phys. 89 (1988) 4600.
[18] K.R. Morgan, S. Collier, G. Burns, K. Ooi, J. Chem. Soc. Chem. Commun. 2 (1994) 1719.
[19] Y.J. Lee, F. Wang, C.P. Grey, J. Am. Chem. Soc. 120 (1998) 12601.
[20] Powder Diffraction File, Card No. 35-0782, ICPDS International Center for Diffraction Data, Swarthmore, PA, USA, 1991.